Electronic Supplementary Material (ESI) for Inorganic Chemistry Frontiers.
This journal is © the Partner Organisations 2021

Supporting Information

Construction of a new $Au_{27}Cd_1(SAdm)_{14}(DPPF)Cl$ nanocluster by surface engineering and insight into its structure-property correlation

Liyun Xu,‡ Qinzhen Li,‡ Tianrong Li, Jinsong Chai, Sha Yang,* and Manzhou Zhu*

Institutes of Physical Science and Information Technology and Centre for Atomic Engineering of Advanced Materials, Key Laboratory of Structure and Functional Regulation of Hybrid Materials of Ministry of Education, Department of Chemistry and Anhui Province Key Laboratory of Chemistry for Inorganic/Organic Hybrid Functionalized Materials, Anhui University, Hefei, Anhui 230601, China

‡L.X and Q.L. contributed equally.

*E-mails of corresponding authors: yangshac@ahu.edu.cn (S. Y.); zmz@ahu.edu.cn (M. Z.).

Notes: The authors declare no competing financial interest.

This Supporting Information includes:

The synthesis of other nanoclusters and complexes

Figures S1-17

Tables S1-2

The synthesis of the nanoclusters including the $Au_{38}(SC_2H_4Ph)_{24}$, $Au_{24}(SAdm)_{16}$, $Au_{22}Cd_1(SAdm)_{16}$, $Au_{22}Cd_1(SAdm)_{15}Br$ were conducted according to procedures reported in the literature,[1-4] and these nanoclusters were obtained as described (Figure S10, 12, 14, and 15).

The syntheses of the Au-SAdm complex were adding 200 μL $HAuCl_4$•$4H_2O$ to 10 mL of ethanol solution, then 75 mg HSAdm was added to into this solution, keeping stiring for two hours. The product was centrifugated to remove the supernatant and washed with methanol for several times.

The syntheses of the Au-DPPF complex were adding 200 μL $HAuCl_4$•$4H_2O$ to 10 mL of ethanol solution, then 55 mg DPPF was added to into this solution, keeping stiring for twelve hours. The product was centrifugated to remove the supernatant and was washed with methanol for several times.

REFERENCES

(1) H.-F Qian, W. T. Eckenhoff, Y. Zhu, T. Pintauer and R.-C. Jin, Total Structure Determination of Thiolate-Protected Au_{38} Nanoparticles, *J. Am. Chem. Soc.*, 2010, **132**, 8280-8281.

(2) D. Crasto, G. Barcaro, M. Stener, L. Sementa, A. Fortunelli, A. Dass, $Au_{24}(SAdm)_{16}$ Nanomolecules: X-ray Crystal Structure, Theoretical Analysis, Adaptability of Adamantane Ligands to Form $Au_{23}(SAdm)_{16}$ and $Au_{25}(SAdm)_{16}$, and Its Relation to $Au_{25}(SR)_{18}$, *J. Am. Chem. Soc.*, 2014, **136**, 14933-14940.

(3) Y.-W. Li, M. J. Cowan, M. Zhou, T.-Y. Luo, Y.-B. Song, H. Wang, N. L. Rosi, G. Mpourmpakis and R.-C. Jin, Atom-by-Atom Evolution of the Same Ligand-Protected Au_{21}, Au_{22}, $Au_{22}Cd_1$, and Au_{24} Nanocluster Series, *J. Am. Chem. Soc.*, 2020, **142**, 20426-20433.

(4) Y.-W. Li, M. J. Cowan, M. Zhou, M. G. Taylor, H. Wang, Y.-B. Song, G. Mpourmpakis and R.-C. Jin, Heterometal-Doped M_{23} (M = Au/Ag/Cd) Nanoclusters with Large Dipole Moments, *ACS Nano*, 2020, **14**, 6599-6606.

(5) S. Zhao, H Zhang, S. D. House, R.-X. Jin, J. C. Yang, and R.-C. Jin, Ultrasmall Palladium Nanoclusters as Effective Catalyst for Oxygen Reduction Reaction, *ChemElectroChem*, 2016, **3**, 1225–1229.

(6) R.-X. Jin, S. Zhao, C. Liu, M. Zhou, G. Panapitiya, Y. Xing, N. L. Rosi, J. P. Lewisd and R.-C. Jin, Controlling Ag-doping in $[Ag_xAu_{25-x}(SC_6H_{11})_{18}]^-$ nanoclusters: cryogenic optical, electronic and electrocatalytic properties, *Nanoscale*, 2017, **9**, 19183–19190.

(7) R. Wang, J.-J. Feng, W.-D. Liu, L.-Y. Jiang, A.-J. Wang, A novel label-free electrochemical immunosensor based on the enhanced catalytic currents of oxygen reduction by AuAg hollow nanocrystals for detecting carbohydrate antigen 199, *Biosensors and Bioelectronics*, 2017, **96**, 152–158.

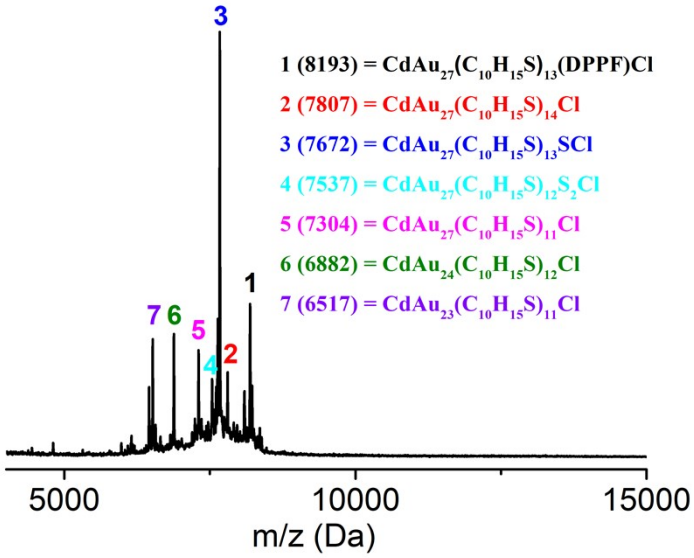

Figure S1. MALDI-MS spectrum of $Au_{27}Cd_1(SAdm)_{14}(DPPF)Cl$ nanocluster.

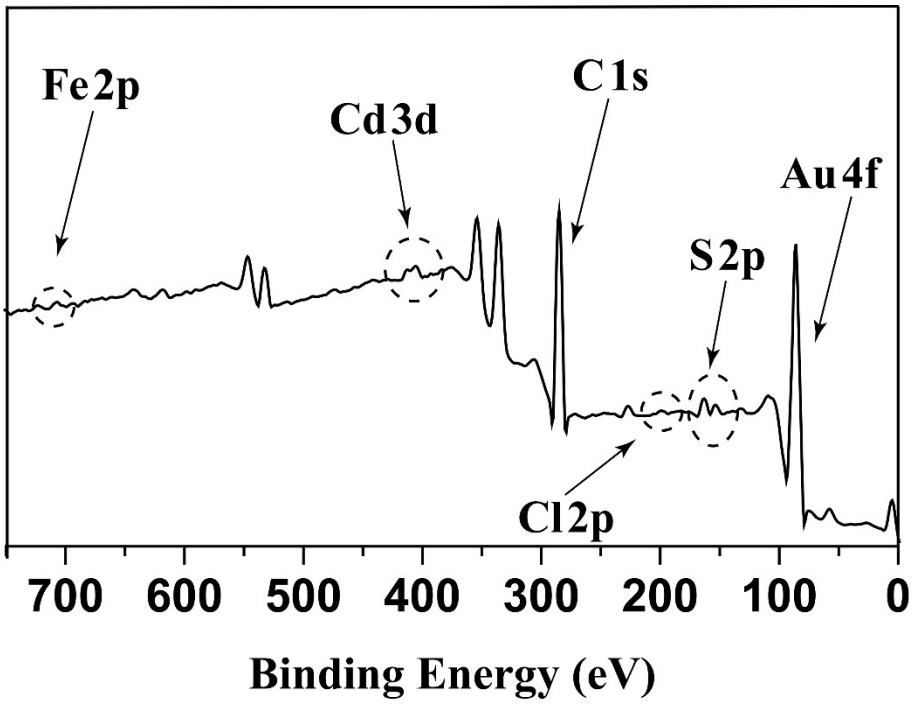

Figure S2. XPS of $Au_{27}Cd_1(SAdm)_{14}(DPPF)Cl$ nanocluster.

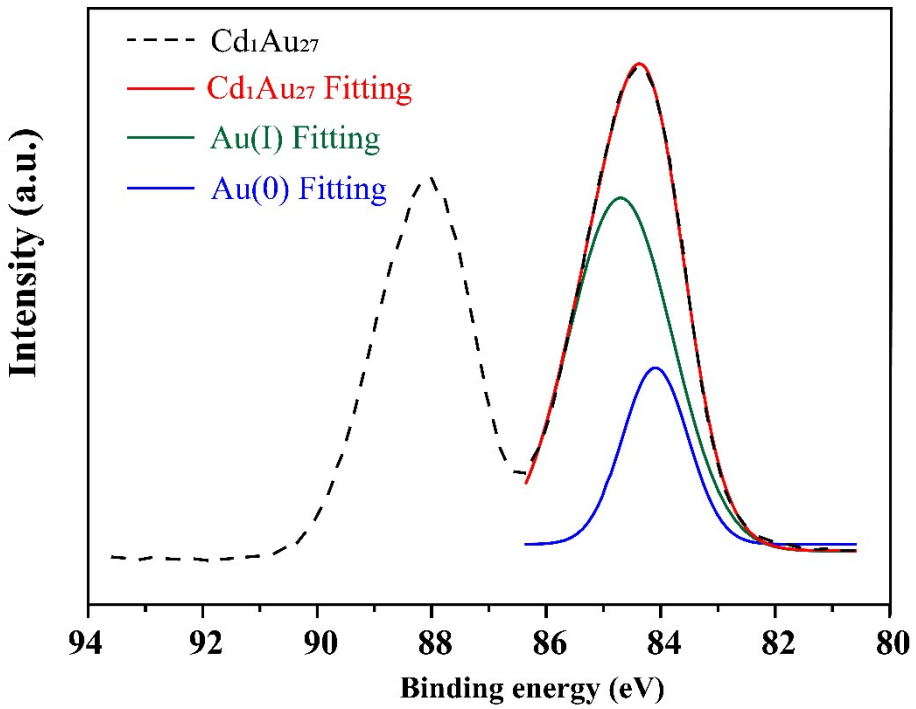

Figure S3. The Au 4*f* spectrum of $Au_{27}Cd_1(SAdm)_{14}(DPPF)Cl$ nanocluster.

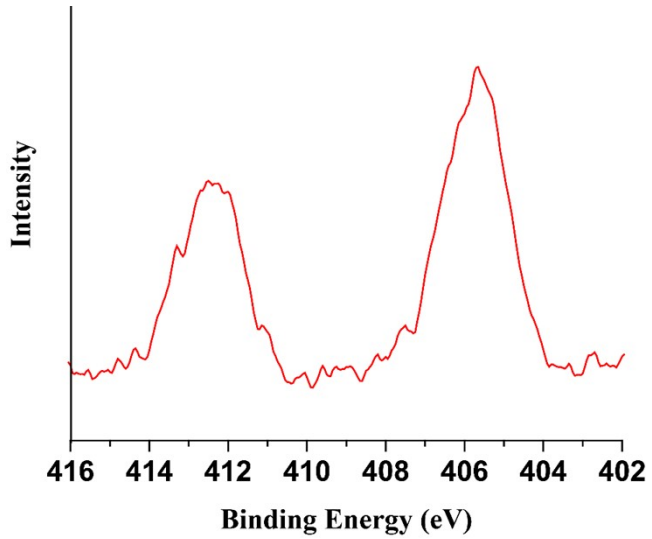

Figure S4. The Cd 3*d* spectrum of $Au_{27}Cd_1(SAdm)_{14}(DPPF)Cl$ nanocluster.

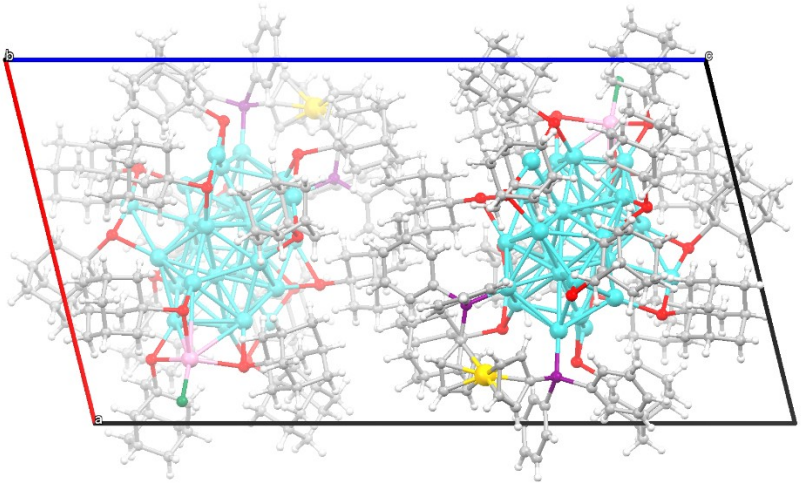

Figure S5. The unit cell of $Au_{27}Cd_1(SAdm)_{14}(DPPF)Cl$ nanocluster (color label: Au = blue; Cd = pink; S = red; P = purple; Fe = yellow; Cl = green; C = gray; H = white).

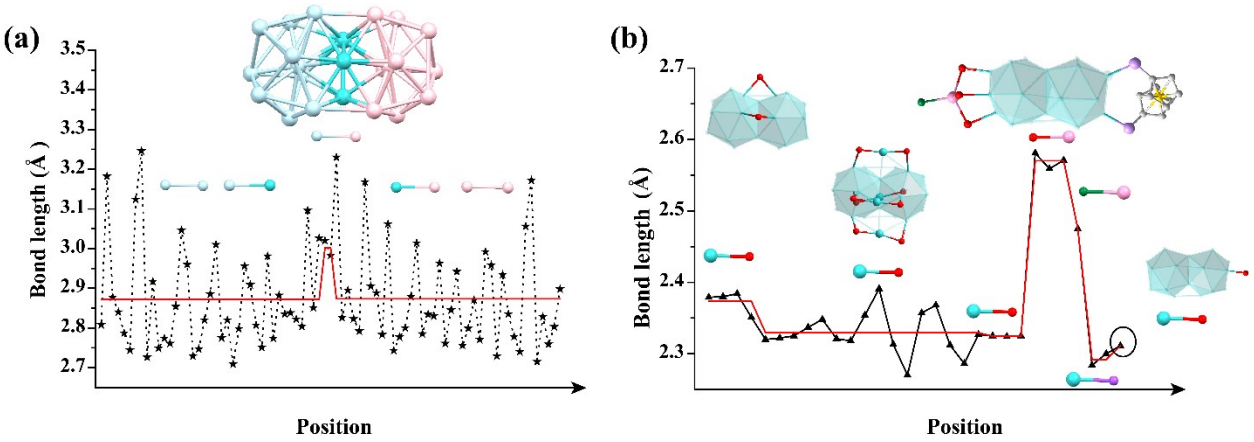

Figure S6. Bond lengths of the (a) Au-Au bonds and (b) M-L bonds of $Au_{27}Cd_1(SAdm)_{14}(DPPF)Cl$ nanocluster (color label: Au = blue; Cd = pink; S = red; P = light purple; Fe = yellow; Cl = green).

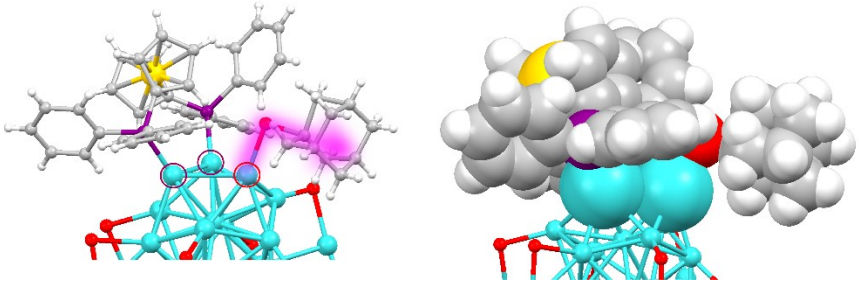

Figure S7. Bottom structure of $Au_{27}Cd_1(SAdm)_{14}(DPPF)Cl$ nanocluster (color label: Au = blue; S = red; P = purple; Fe = yellow; C = gray; H = white).

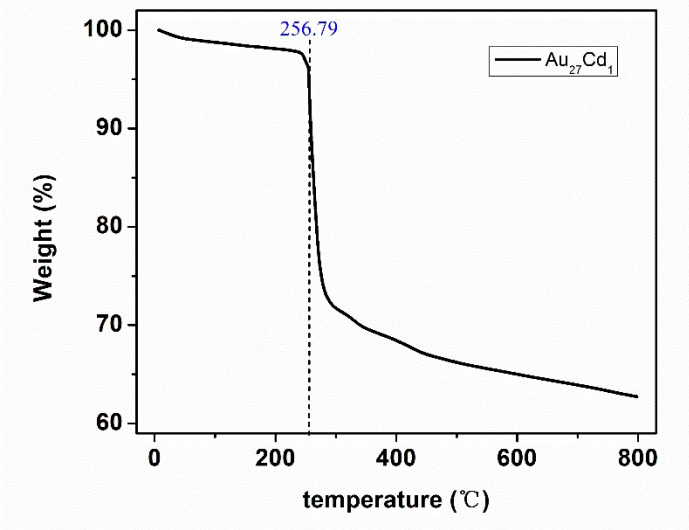

Figure S8. TGA curve of $Au_{27}Cd_1(SAdm)_{14}(DPPF)Cl$ nanocluster.

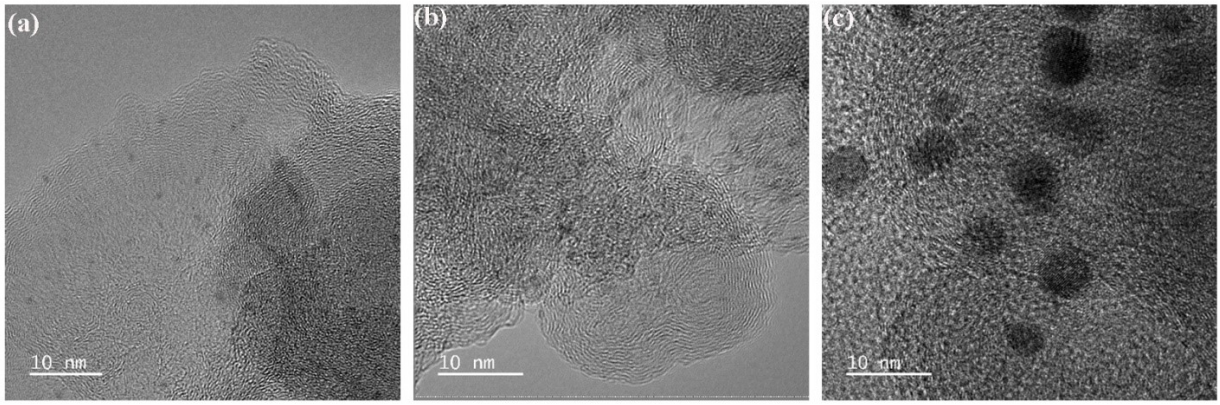

Figure S9. TEM images of $Au_{27}Cd_1(SAdm)_{14}(DPPF)Cl/C$ before (a) and after calcination at 150 ℃ (b) and 300 ℃ (c).

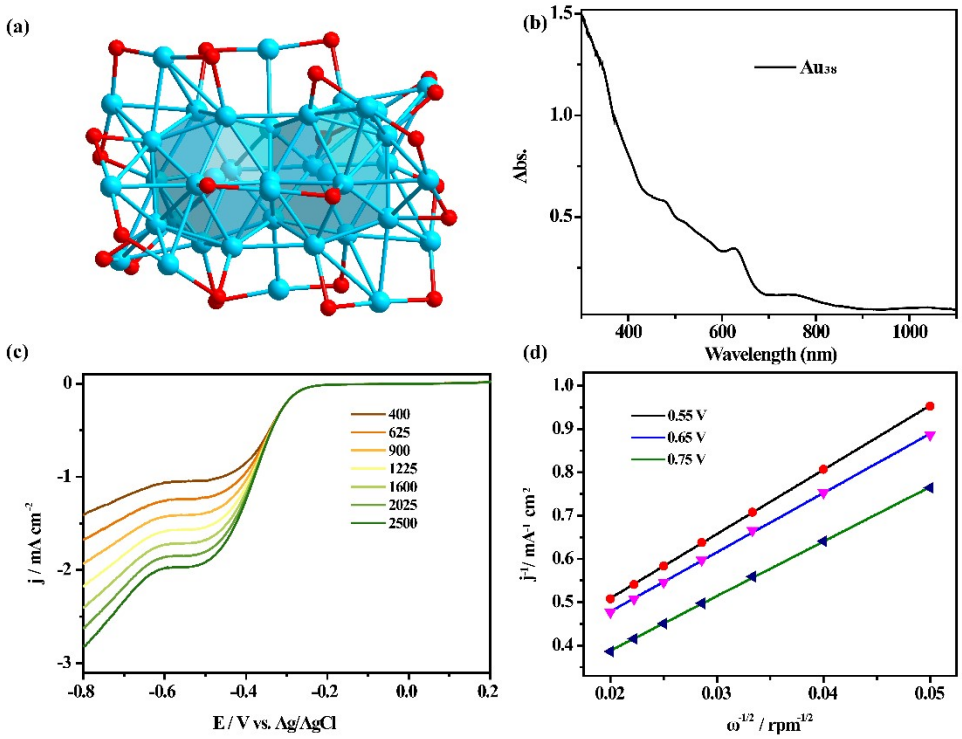

Figure S10. (a) The framework structure and (b) UV-vis spectrum of $Au_{38}(SC_2H_4Ph)_{24}$ nanocluster. (c) RDE voltammograms of $Au_{38}(SC_2H_4Ph)_{24}$/C catalyst at different rotating speeds in O_2-saturated 0.1 M KOH solutions. (d) Koutecky-Levich plots (j^{-1} vs. $\omega^{-1/2}$) of $Au_{38}(SC_2H_4Ph)_{24}$/C catalyst at different potentials.

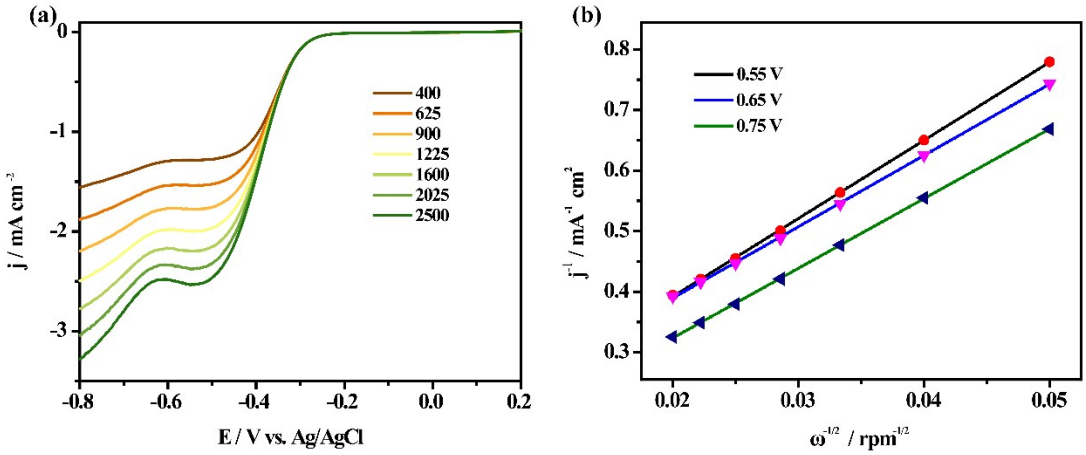

Figure S11. (a) RDE voltammograms of Au-SAdm/C catalyst at different rotating speeds in O_2-saturated 0.1 M KOH solutions. (b) Koutecky–Levich plots (j^{-1} vs. $\omega^{-1/2}$) of Au-SAdm/C catalyst at different potentials.

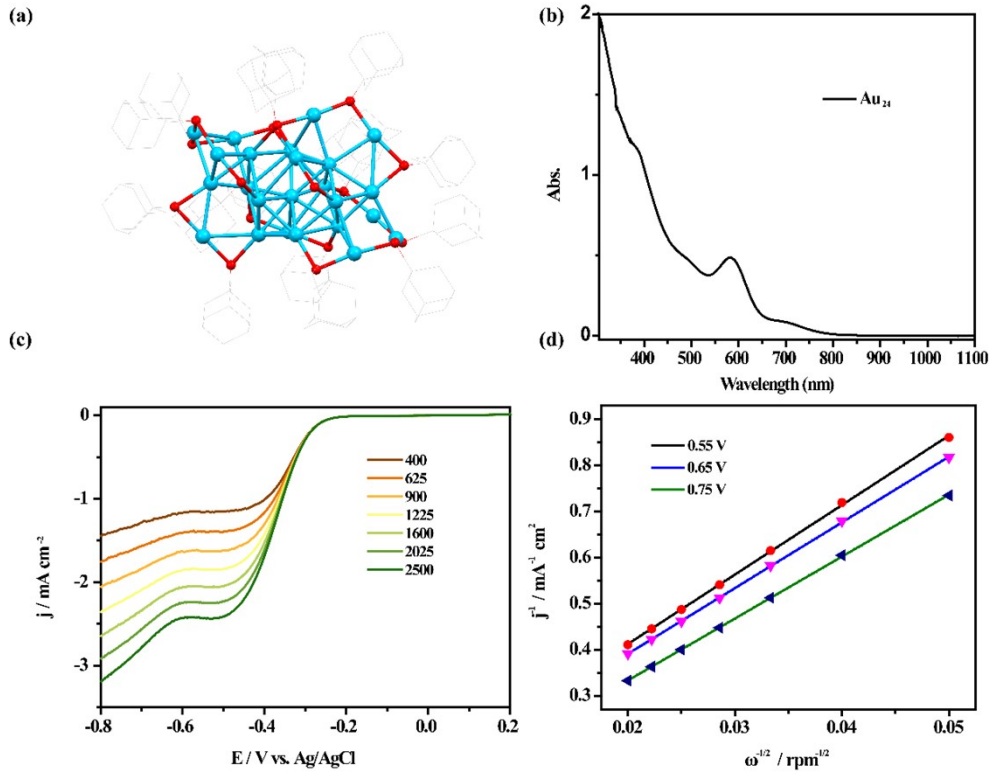

Figure S12. (a) The crystal structure and (b) UV-vis spectrum of $Au_{24}(SAdm)_{16}$ nanocluster. (c) RDE voltammograms of $Au_{24}(SAdm)_{16}$/C catalyst at different rotating speeds in O_2-saturated 0.1 M KOH solutions. (d) Koutecky–Levich plots (j^{-1} vs. $\omega^{-1/2}$) of $Au_{24}(SAdm)_{16}$/C catalyst at different potentials.

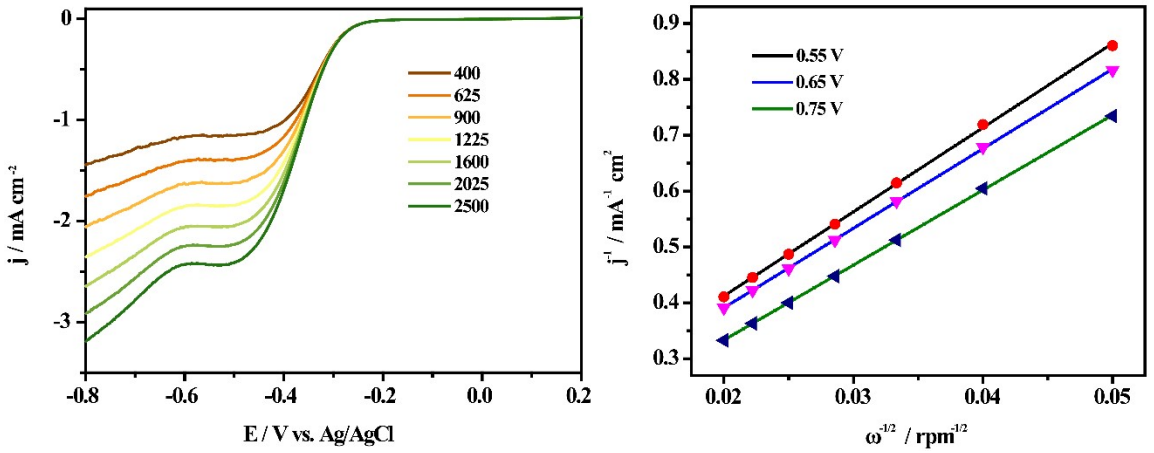

Figure S13. (a) RDE voltammograms of Au-DPPF/C catalyst at different rotating speeds in O_2-saturated 0.1 M KOH solutions. (b) Koutecky–Levich plots (j^{-1} vs. $\omega^{-1/2}$) of Au-DPPF/C catalyst at different potentials.

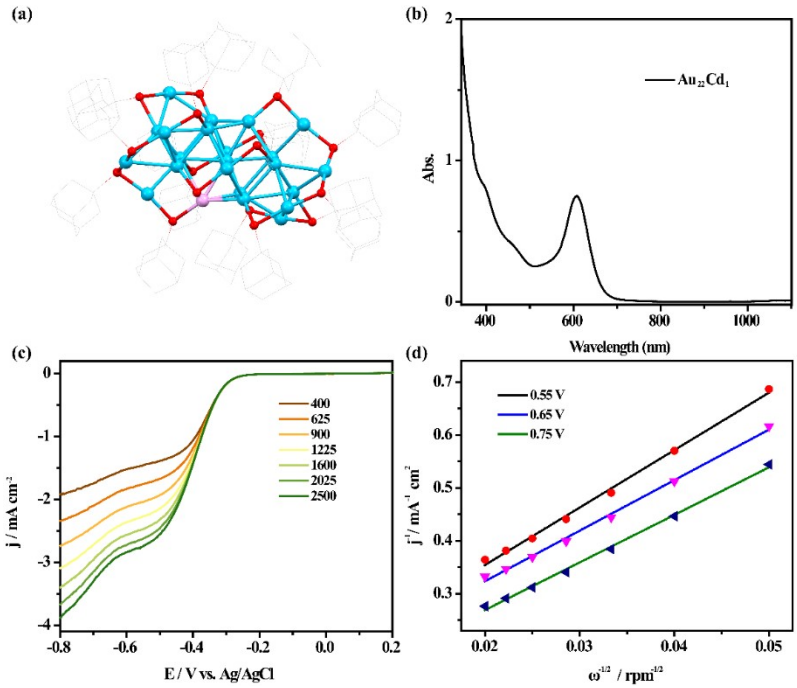

Figure S14. (a) RDE voltammograms of $Cd_1Au_{22}(SAdm)_{16}$/C catalyst at different rotating speeds in O_2-saturated 0.1 M KOH solutions. (b) Koutecky–Levich plots (j^{-1} vs. $\omega^{-1/2}$) of $Cd_1Au_{22}(SAdm)_{16}$/C catalyst at different potentials.

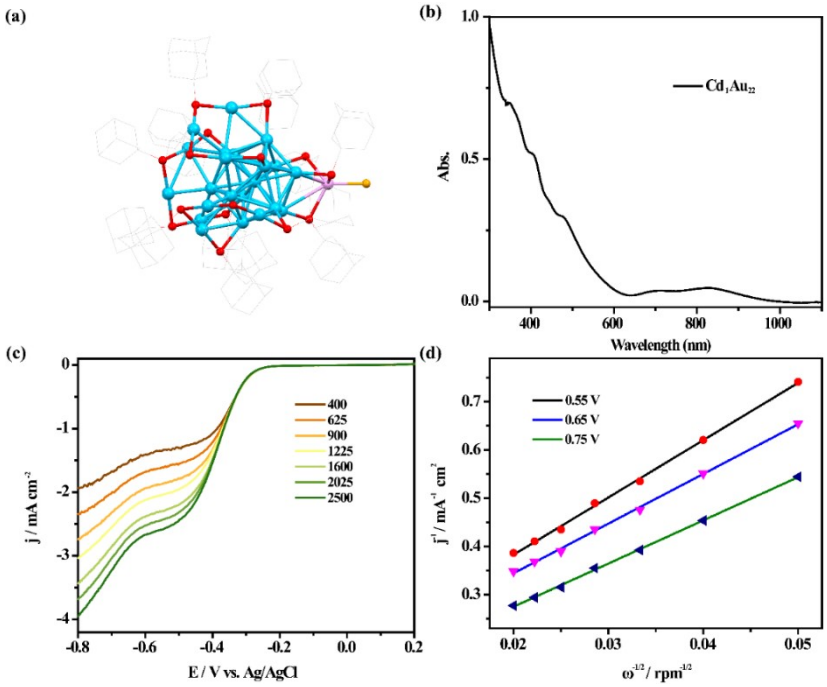

Figure S15. (a) The crystal structure and (b) UV-vis spectrum of $Cd_1Au_{22}(SAdm)_{16}Br$ nanocluster. (c) RDE voltammograms of $Cd_1Au_{22}(SAdm)_{16}Br$/C catalyst at different rotating speeds in O_2-saturated 0.1 M KOH solutions. (d) Koutecky–Levich plots (j^{-1} vs. $\omega^{-1/2}$) of $Cd_1Au_{22}(SAdm)_{16}Br$/C catalyst at different potentials.

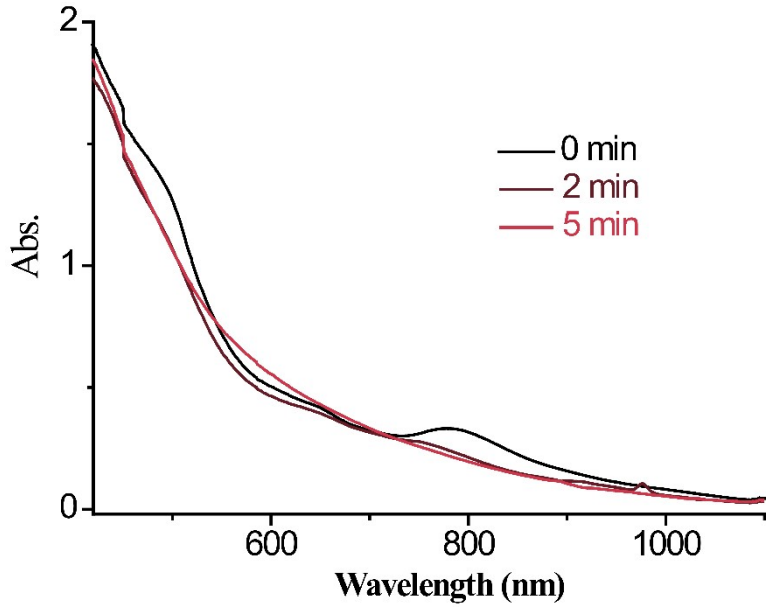

Figure S16. The reducing stability test of the $Au_{27}Cd_1$ nanocluster.

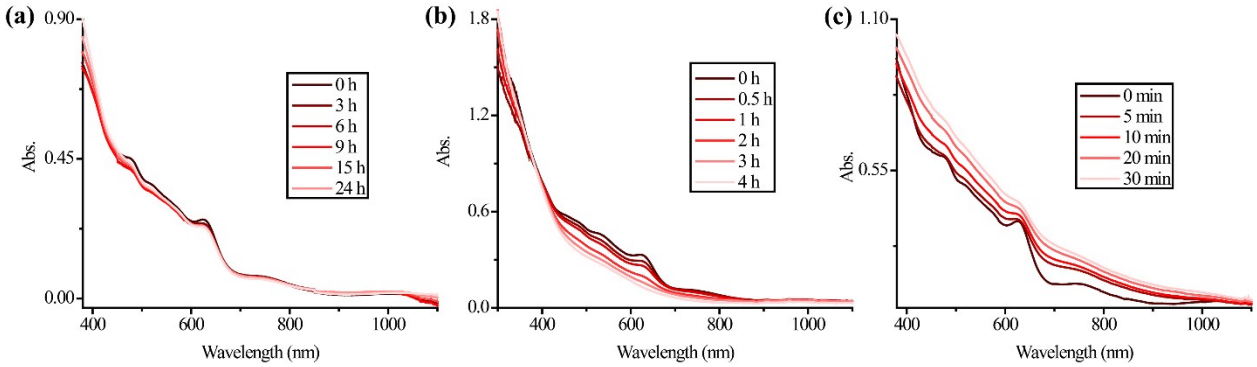

Figure S17. (a) the thermal stability test (b) the oxidizing stability test and (c) the reducing stability test of the Au_{38} nanocluster.

Table S1. Comparison of the ORR activities of different samples calculated by LSV measurements in 0.1 M KOH solution.

Sample	E_{onset} (V)	$E_{1/2}$ (V)	j_p(mA cm^{-2}) at -0.8 V	number of electrons transferred	H_2O yield	H_2O_2 yield
$Au_{27}Cd_1(SAdm)_{14}(DPPF)Cl/C$	-0.16	-0.41	4.25	3.3	65%	35%
$Au_{38}(SC_2H_4Ph)_{24}/C$	-0.17	-0.40	2.39	2.0	0	100%
Au-SAdm/C	-0.17	-0.40	2.78	2.2	10%	90%
$Au_{24}(SAdm)_{16}/C$	-0.17	-0.38	2.71	2.2	10%	90%
Au-DPPF/C	-0.16	-0.38	2.64	2.0	0	100%
$Cd_1Au_{22}(SAdm)_{16}/C$	-0.19	-0.42	3.39	3.0	50%	50%
$Cd_1Au_{22}(SAdm)_{16}Br/C$	-0.18	-0.42	3.43	2.9	45%	55%
$Pd_{13-17}(SR)_{18-22}/C$[5]	-0.02	-	-	3.9	95%	5%
$[Ag_xAu_{25-x}(SC_6H_{11})_{18}]^-/C$[6]	-0.09	-	-	3.0	50%	50%
AuAg hollow NCs/C[7]	-0.09	-	-	3.99	99.5%	0.5%

The onset potential (E_{onset}), half-wave potential ($E_{1/2}$), and j_p were determined from rotating disk voltammograms with a rotation speed of 1600 rpm at -0.8 V.

Table S2. Crystal data and structure refinement for $Au_{27}Cd_1(SAdm)_{14}(DPPF)Cl$ nanocluster.

CCDC	2045434
Empirical formula	$C_{174}H_{238}Au_{27}CdClFeP_2S_{14}$
Formula weight	8362.21
Temperature/K	293(2)
Crystal system	triclinic
Space group	P-1
a/Å	18.1614(8)
b/Å	20.2561(9)
c/Å	31.4539(14)
α/°	87.030(4)
β/°	76.077(3)
γ/°	67.765(3)
Volume/Å^3	10386.2(8)
Z	2
ρ_{calc}g/cm^3	2.674
μ/mm^{-1}	38.035
F(000)	7520.0
Radiation	Cu Kα (λ = 1.54186)
2Θ range for data collection/°	6.922 to 124.994
Index ranges	$-20 \leq h \leq 18$, $-23 \leq k \leq 17$, $-36 \leq l \leq 23$
Reflections collected	72576
Independent reflections	32175 [R_{int} = 0.0891, R_{sigma} = 0.1496]
Data/restraints/parameters	32175/555/1231
Goodness-of-fit on F^2	0.937
Final R indexes [I>=2σ (I)]	R_1 = 0.0742, wR_2 = 0.1949
Final R indexes [all data]	R_1 = 0.1186, wR_2 = 0.2091
Largest diff. peak/hole / e Å^{-3}	3.78/-2.75